EREM 78/2
Journal of Environmental Research, Engineering and Management
Vol. 78 / No. 2 / 2022
pp. 118–128
DOI 10.5755/j01.erem.78.2.29971

Modeling the Atmospheric Stability and the Mixing Layer Depth and their Relationship with Sandstorms in an Arid Area

Received 2021/10 | Accepted after revision 2022/05

http://dx.doi.org/10.5755/j01.erem.78.2.29971

Modeling the Atmospheric Stability and the Mixing Layer Depth and their Relationship with Sandstorms in an Arid Area

Saud Jaza Almutairi
Department of Civil Engineering, College of Engineering, Qassim University, Unaizah, Saudi Arabia

Ragab ElSayed Rabeiy*
Department of Civil Engineering, College of Engineering, Qassim University, Unaizah, Saudi Arabia
Leave from Faculty of Engineering, Assiut University, Assiut, Egypt

***Corresponding author:** r.elsayed@qu.edu.sa

The atmospheric stability and depth of the mixing layer are essential parameters in modelling the dispersion of pollutants and sandstorms in arid regions. In this study, a MATLAB model was used to determine the hourly atmospheric stability conditions and the depth of the mixing layer in the year 2019, especially during sandstorms events. The statistical analysis of hourly sandstorms was investigated over four decades (from 1980 to 2019) and its relationships with the weather conditions, especially wind speed and direction were figured in the study area. The average mixing layer during daytime hours in the summer season was 1800 ± 400 m, while during night hours, the average mixing height was 500 ± 200 m. The study concluded that the major wind direction during sandstorms was blowing to the south direction ± 22.5 degrees. It was noted that relative humidity increased while the average temperature decreased over the last decade during the sandstorm events due to the wide cultivation in this period. The cultivation of tall trees on the northwest side of the study area will decrease the severity of sandstorms in future. This study could be applied to arid regions that suffer sandstorms such as Arabian Peninsula.

Keywords: mixing height, atmospheric stability, sandstorms, arid areas, wind regime.

Introduction

One of the most important meteorological input parameters into air pollution models is the atmospheric boundary layer or mixing height (Brokamp et al., 2019). The boundary layer is the layer where interactions occur between the Earth's surface and the wide scale of atmospheric flow (Wang et al., 2019). Pollutants are mixed in different manners throughout this layer by turbulence (Levi et al., 2020). Turbulent mixing can be either convective due to solar energy and/or mechanical via wind movement. Convection occurs during the daytime, when surface air is heated via the solar energy that transfers from Earth's surface air parcel (Schumann, 1988). Mechanical turbulence results from the shearing forces formed when the wind blows over Earth's surface (Tanamachi et al., 2019). As the wind speed increases, mechanical turbulence increases and is larger over rough surface than over smooth surface (Honnert et al., 2020).

Sandstorms are weather conditions that usually occurr in arid and semiarid regions where low precipitation and high temperature are the main features (Albugami et al., 2019). These conditions happen because of intense winds which activate fine sand from bare areas and carry it for large distances over the surrounding areas (Butt & Mashat, 2018). The fine particles of sandstorms are inhaled by individuals, enter the respiratory device and cause health problems in the lungs such as asthma. The diseases of the respiratory system induced by air pollutants are influenced by the type of minerals, grain size, and duration of exposure to these particles (Samarkandi et al., 2017).

Several studies investigated the sandstorms in and around this study area. Alharbi and Gomaa (2014) collected dust samples that deposited during sandstorms from 18 different sites in Qassim region during 2012 and 2013. They analysed the size distribution and the physio-chemical properties of dust fall. The results showed that the composition of the collected dust samples was mainly loamy sand and clay (44.5% sand, 27.4% silt and 28.19% clay). Also, the collected samples contained considerable concentration of trace elements such as Pb, Zn, and Mn. Modaihsh et al. (2017) collected dust samples using a marble dust collector from 15 sites within Riyadh city during the year 2012. The samples were analysed to detect the composition of dust that falls from the dust storms. Also, they estimated the average monthly amount of dust fall from the dust storms which was 14.5 tons per km^2 in Riyadh airport. Beegum et al. (2018) studied seven sandstorm events from the year 2014 to 2017 over the Arabian Peninsula. They investigated the impacts of the dust storms on the horizontal visibility and air quality. The horizontal visibility during the dust storms decreased to near-zero coincident with worst air quality. Albaqami (2020) analysed meteorological data measured from 27 stations in Saudi Arabia and investigated the spatial and temporal distribution of dust storms from the year 2000 to 2016. The study proved a significant positive relationship ($p < 0.005$) between dust storms and high wind speed. According to her statistical analysis, the events of dust storms were decreasing in recent years over the northern areas such as Qassim region. Soltan et al. (2020) collected dust samples during sandstorms at Ar Rass city, Qassim, Saudi Arabia. They analysed the chemical composition of the collected samples such as Cd, Co, Cr, Cu, Fe, Mn, Ni, Pb and Zn. The impacts of dust fall on human health, cultivated lands, plant growth, and groundwater were investigated. The major components found on the collected samples were aluminosilicate, SiO_2 and $CaCO_3$, and considerable values of cadmium and nickel. They did not study the wind direction and wind velocity over a long-time scale during sandstorms. Also, no previous studies addressed the atmospheric stability and the height of the mixing layer during the hours of sandstorms.

The objectives of this work were to (1) estimate the Pasquill–Gifford hourly atmospheric stability categories, the height of the mixing layer and atmospheric factors such as convective velocity and friction velocity, (2) investigate the sandstorms' behaviour based on the estimated atmospheric stability conditions and mixing height, (3) analyse the wind speed and wind direction during sandstorms along four decades, and (4) suggest control methods to decrease the severity

of sandstorms based on the results of the model and statistical analysis of dust storms over four decades.

Materials and Methods

Study area and used data

The study was applied in Qassim region, Saudi Arabia (KSA). The study area is one of the thirteen provinces of KSA that is located at (26.0°–26.2°) N and (43.98°–44.2°) E with an average elevation of 670 m relative to sea level. The dunes and the desert around the study area are characterized by very low amounts of precipitation and sparse natural vegetation cover that periodically creates sandstorms during windy hours (Abolkhair, 1986). A MATLAB code that was developed by Rabeiy (2010) was modified to suit the sandstorm events. The modified code determines the hourly atmospheric stability categories, the height of the mixing layer, the friction velocity, and the convective velocity based on the surface meteorological data. The weather data used are surface temperature, barometric pressure, incoming solar radiation, percentage of cloud cover, wind speed, and wind direction. The weather data includes hourly recorded values over the year 2019 with total rows of 8760, each row containing 15 columns. Two columns of the data record the hourly sandstorm events. Additional to the surface weather data, the study used hourly events of sandstorms over four decades (from 1980 to 2019) to investigate the wind direction wind speed during dust storm events. Wind rose and histogram were produced using WRPLOT View, Version 8.0.2 freeware available in Lakes Environment. Tables and other figures were generated using Microsoft Office.

Theory of the model

The amount of turbulence is categorized into stability classes. The most widely used categories are the Pasquill-Gifford stability classes A, B, C, D, E, and F (Morbidelli et al., 2011; Zaïdi et al., 2014). Atmospheric stability classes A, B, and C occur during daytime hours. Class A is the very unstable conditions, while stability class B is moderately unstable conditions and class C is slightly unstable conditions. Class D of atmospheric stability refers to the condition of a neutral atmosphere (Zaïdi et al., 2014). Neutral atmospheric conditions may coincide either during the daytime hours or during night hours. Stability classes E and F occur only in night hours when low energy reaches the Earth's surface. Class E is a stable condition while class F refers to the most stable condition (Schutt et al., 2015).

The depth of the mixing layer at any study area can be found using experimental methods or mathematical methods. It is estimated experimentally by measuring wind speed and temperature at different altitudes. The techniques of these experiments use radiosonde, sodar, clear-air radar, and LIDAR (Tangborn et al., 2020). The experimental methods are not accessible at the study area location. The other probability is the use of mathematical models based on the measured surface weather elements. Many studies (Benkley & Schulman, 1979) used mathematical models to determine the mixing layer height. The model used to calculate the height of the mixing layer in the cases of unstable conditions (A, B and C stability classes) is proposed as in equation (1).

$$H_m = -0.4L\left(\frac{\omega_*}{U_*}\right)^3 \quad (1)$$

The mixing height depends on the mechanical and convective turbulence values during the daytime. During the night, mechanical turbulence predominates. Neutral conditions occur during the day or the night when the sky is covered by heavy clouds; therefore, convective turbulence is neglected, and mechanical effect is only considered. Equation (2) (Benkley & Schulman, 1979) is recommended to estimate the depth of the mixing layer in case of neutral conditions, which is also given by Baklanov (2004).

$$H_m = 0.185\frac{U_*}{f} \quad (2)$$

Stable conditions E and F are night-time conditions, which means that convective force does not exist. The cap of the mixing height for stable conditions is explained as the height at which turbulence fades, and above it the effects of sensible heat and shear stress can be neglected (Yu, 1978). Arya (1981) proposed the equation (3) to calculate the nocturnal height of the mixing layer.

$$H_m = 113.5 + 0.34\left(\frac{LU_*}{f}\right)^{1/2} \quad (3)$$

Where H_m is the mixing height, L is the Monin-Obukhov length, U_* is the friction velocity, f is the Coriolis factor, and ω_* is the convective velocity. Factor f is called Coriolis factor which is estimated as given in equation (4), where ω is the rate of Earth's rotation and the angle ϕ is the latitude of the study area (Hutter et al., 2011).

$$f = 2\omega \sin\phi \quad (4)$$

Results and Discussion

Analysis of the measured weather data

The wind speed and its directions were analysed using the plot of wind rose with a histogram, as indicated in *Figs. 1(a)* and *1(b)* in the year 2019. The average wind speed in the study area was found to be 3.6 m/s, with a maximum of 16.5 m/s. The wind speed is 48.4% less than 3 m/s during the night-time hours. An increasing wind speed during the night-time hours enhances the mechanical turbulence in the atmosphere, which increases the mixing depth. Wind direction is important to be analysed to decide the directions of pollutants in the atmosphere and blowing dust during sandstorms. As indicated in the *Fig. 1(a)*, the wind direction is mainly from the north and the northeast, with significant values from the north. The diurnal variation in wind speed is illustrated in *Fig. 2(a)*, which illustrates that the wind speed is greater during night-time hours in spring season.

The study area is in the middle of KSA in an arid area with high temperatures in the summer and low temperatures in the winter, especially at night. The temperature in the summer reaches 46°C with an average value of 36°C. In winter season, the minimum recorded temperature is 3.5°C with an average value of 16°C. Diurnal recorded temperature during the four seasons is presented in *Fig. 2(b)*. The maximum recorded solar radiation during the summer daytime hours exceeded 1250 W/m^2, while the maximum in winter was 1078 W/m^2. The diurnal recorded incoming solar energy on the surface in W/m^2 is presented in *Fig. 2(c)*. The increasing incoming solar radiation in the summer

Fig. 1(a). *Wind rose diagram presents the directions and percentage of prevailing wind during the year of 2019 in the study site*

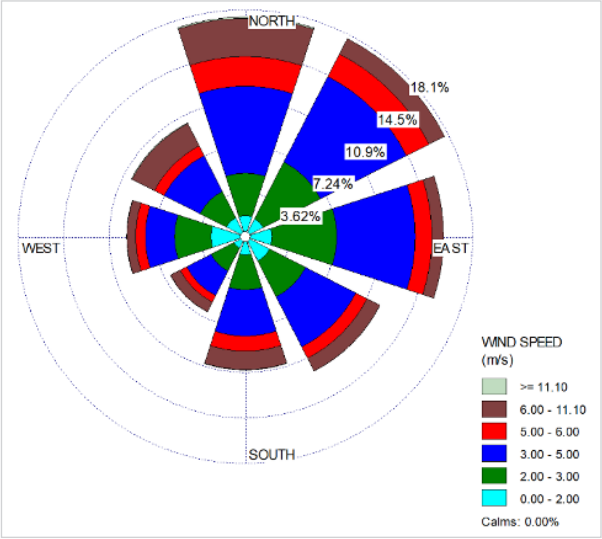

Fig. 1(b). *Wind speed histogram with classes meeting Pasquill stability categories*

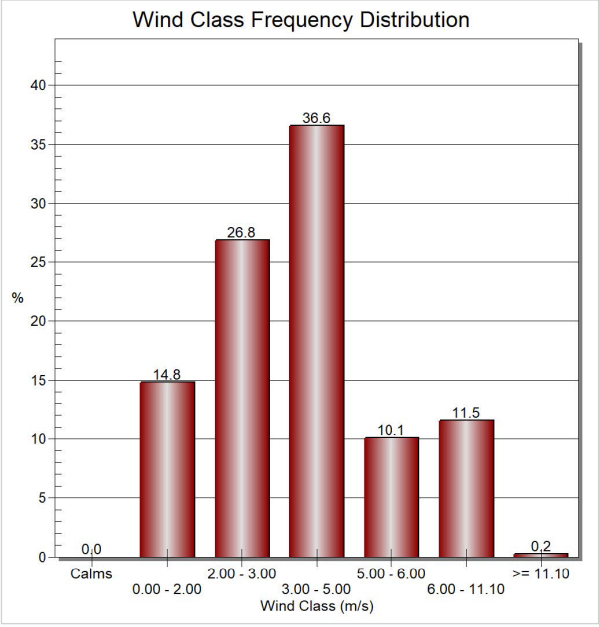

satisfies the requirement of the unstable atmospheric conditions (A, B and C classes). Unstable conditions increase the dispersion and dilution of contaminants in the low layer of the ground. The climate in the study area features low humidity most of the year, with an average of 65% in winter and 21% in summer, with a maximum value of 43% in summer.

Fig. 2(a). *Diurnal variation in wind speed*

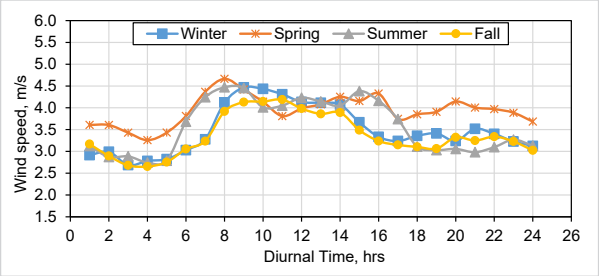

Fig. 2(b). *Diurnal variation in temperature*

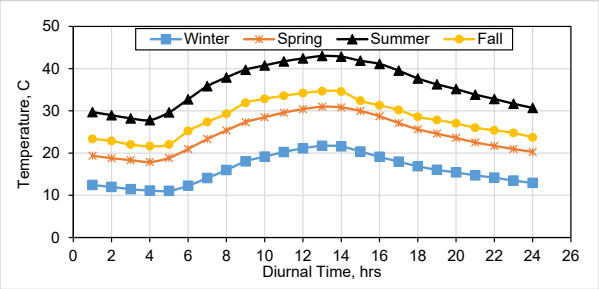

Fig. 2(c). *Diurnal variation in incoming solar radiation*

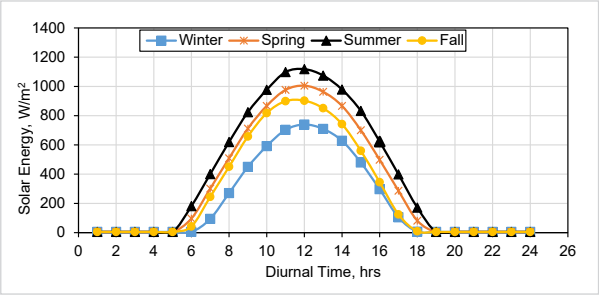

Results and Discussion of the Developed Model

The developed model utilizes surface weather data to estimate atmospheric stability according to the classification of Pasquill-Gifford as given in *Table 1* (Gifford Jr, 1961). Stability near the ground depends on the net radiation as an indication of convective turbulence and on wind speed, which refers to mechanical turbulence. Incoming solar radiation (insolation) depends on the angle of solar elevation (h°) and the amount of cloud cover (Latini et al., 2000). The class of incoming solar radiation is considered strong, moderate, or slight if the solar elevation angle is greater than 60°, between 35° and 60°, or less than 35°, respectively, as described in *Table 2* (Barratt, 2002). The model utilized the recorded incoming solar radiation instead of solar elevation angle and cloud cover to determine the strength of insolation. The suggested values of incoming solar radiation to match the amount of insolation strength are as follows: larger than 1000 (W/m^2) assigned for strong insolation; the values from 1000 to 700 (W/m^2) assigned for moderate insolation; the values from 700 to 400 (W/m^2) assigned for slight insolation; and less than 400 (W/m^2) assigned for weak insolation, as shown in *Table 2*.

Based on the suggested values of the measured incoming solar radiation and the range of wind speed, the modified MATLAB code determines the hourly atmospheric stability conditions in the study area in year 2019 as illustrated in *Table 3*. The results of the atmospheric stability categories are classified into summer, winter, and the complete year, as presented in *Table 4*.

Table 1. *Meteorological conditions define the Pasquill-Gifford stability categories (Gifford Jr, 1961)*

Surface wind speed	Daytime incoming solar radiation (Insolation)			Night-time cloud cover	
m/s	Strong	Moderate	Slight	> 50%	< 50%
< 2	A	A–B	B	E	F
2–3	A–B	B	C	E	F
3–5	B	B–C	C	D	E
5–6	C	C–D	D	D	D
> 6	C	D	D	D	D

Note: Class D applies to heavily overcast skies, at any wind speed, day or night

Table 2. *Range values of incoming solar radiation match the degree of insolation strength*

Insolation strength	Solar elevation angle (Latini et al., 2000)	Suggested incoming solar range, (W/m^2)	Percentage of recorded data according to solar elevation angle
Strong	$60^\circ < \phi$	> 1000	17.31% larger than 1000 (W/m^2)
Moderate	$35^\circ < \phi \leq 60^\circ$	1000–700	27.60% moderate
Slight	$15^\circ < \phi \leq 35^\circ$	700–400	24.11% slight insolation
Weak	$\phi \leq 15^\circ$	< 400	8.98% weak insolation

In summer, atmospheric stability was found to vary between the very unstable and stable classes. However, in winter, the atmosphere is more stable for longer periods. During winter daytime hours, the neutral condition was dominant with a frequency of 43%, while the atmosphere had a value of only 4.6% for very unstable conditions (category A). On summer days, the frequency of the unstable conditions of the atmosphere increased to 78%. *Table 4* also illustrates that in summer nights the atmosphere is generally stable with a percentage of 86%, while it is 76% in winter due to cloud cover, which increases the chance of neutral conditions. As expected, neutral atmospheric stability is dominant for the overall results with a frequency of 27%.

The hourly height of the mixing layer, the convective velocity, and the friction velocity are estimated by the developed MATLAB code according to the determined atmospheric categories and other recorded weather data. During the daytime, the mixing height is made by both convective turbulence from high surface heating and mechanical turbulence via wind movement. During the night, the height of the mixing layer is controlled only by mechanical turbulence from wind. The diurnal variation in the modelled height of the mixing layer and metrological variables are presented in *Figs. 3, 4* and *5*.

From *Figs. 2* and *3*, it is concluded that the estimated values of mixing height are matching the values of wind speed during the night hours; as the wind speed increases the depth of the mixing layer increases. The diurnal wind speed in the spring night hours is higher than that of the other seasons (*Fig. 2*). It is also noticed that the estimated mixing height and friction velocity in spring night hours are higher than those of the other seasons (*Figs. 3* and *4*). In addition, the relationship between the recorded incoming solar radiation values is obvious with the modelled mixing height and convective velocity during daytime hours. The average mixing height in summer was 2600 m, whereas in winter, the mean value was 1700 m.

The friction velocity depends mainly on the wind speed, while the convective velocity is more related to the surface heat flux calculated from the measured solar radiation. From *Fig. 2*, we note that the friction velocity in spring is greater than that in the other seasons during the night-time, while the convective velocity in summer is greater than that of the other seasons during the daytime.

Table 3. *Classes of atmospheric stabilities according to ranges of wind speed and measured solar radiation fed to the model*

Wind speed, (m/s)	Daytime Measured solar radiation (W/m²)				Nighttime cloud cover	
	> 1000	1000–700	700–400	< 400	≥ 50%	< 50%
< 2	A	A	B	D	E	F
2–3	A	B	B	D	E	F
3–5	B	B	C	D	D	E
5–6	C	C	D	D	D	D
> 6	C	D	D	D	D	D

Table 4. *Results of hourly atmospheric stability categories, %*

Stability Category	Whole Year			Summer Season			Winter Season		
	Days	Nights	All Year	Day	Night	All Summer	Day	Night	All Winter
A	11.2	–	5.4	13.8	–	8.6	4.6	–	2.0
B	35.6	–	17.2	29.1	–	18.2	35.3	–	10.2
C	19.9	–	9.6	35.3	–	13.0	17.3	–	28.6
D	33.4	21.0	27.0	21.8	13.5	20.0	42.9	21.7	14.9
E	–	35.7	18.4	–	36.5	16.9	–	36.0	20.4
F	–	43.3	22.4	–	50.0	23.3	–	42.3	23.9

Fig. 3. *Diurnal variation in the mixing height*

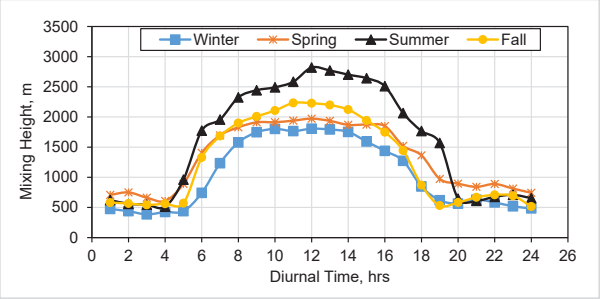

Fig. 4. *Diurnal variation in the friction velocity*

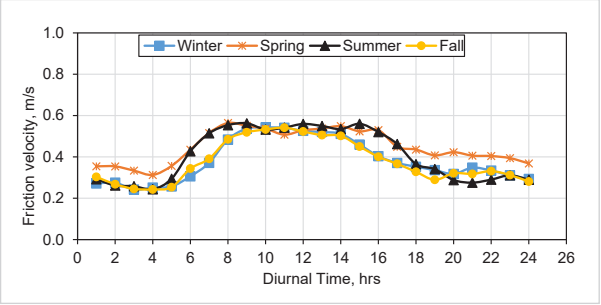

Fig. 5. *Diurnal variation in the convective velocity*

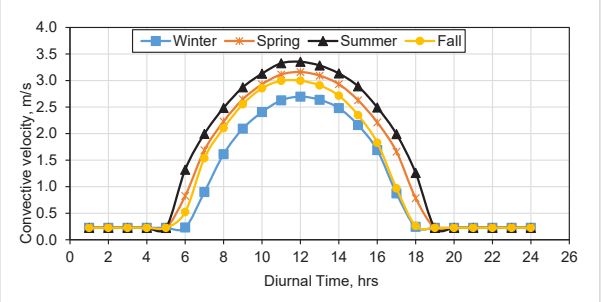

To investigate the changes in the height of the mixing layer according to atmospheric stability conditions, the ranges of the mixing height were developed based on each category of atmospheric stability from A to F stability conditions, as given in *Table 5*. The height of the mixing layer was organized in bands of 200-m intervals against the percentage distributions for each band with the corresponding category of atmospheric stability. The greatest major feature of the distributions is the increase in percentage of higher and lower mixing height values with the alteration based on atmospheric conditions from unstable to stable categories. Based on *Table 5*, 80% of the mixing height in summer was greater than 2100 m in very unstable atmospheric conditions, while for stability category B, 33% of the modelled values of the mixing height were greater than 2100 m, and only 12% of the values were greater than 2100 m. For stable conditions, 86% of the estimated height of the mixing layer was less than 500 m for stability category E and 88% for stability category F. For category D (neutral conditions), a considerable percentage of the mixing height occurred in the range from 1300 m to 1500 m in winter season and summer season, respectively.

The estimated values of the hourly mixing height were also analysed based on incoming solar radiation for the hours of daytime, as indicated in *Fig. 6*. From this figure, we noted that the depth of the modelled mixing layer decreases with decreasing strength of insolation. For solar radiation > 750 (W/m^2), 65% of the mixing height is greater than 2000 m. When incoming solar radiation is less than 250 (W/m^2), only 11% of the calculated mixing heights are greater than 2000 m. Additionally, 20%, 11%, and 7% of the estimated values of mixing heights are larger than 2000 m for classes > 750 (W/m^2), (750–250) (W/m^2), and < 250 (W/m^2), respectively.

The modelled height of the mixing layer was investigated according to the ranges of wind speed during night-time hours, as indicated in *Fig. 7*. From this figure, we can conclude that the mixing height decreases with decreasing wind speed. When wind speed is > 5 m/s, all the modelled values of the mixing height are greater than 1700 m. While for calm wind speed (< 2 m/s), the calculated heights of the mixing layer are

Fig. 6. *Ranges of the mixing layer according to the ranges of incoming solar radiation: (> 750), (750–250), and (> 250) W/m^2*

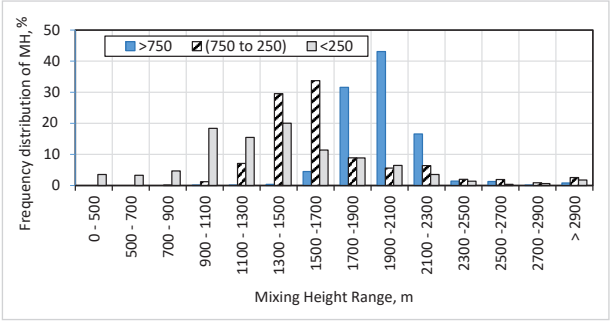

Table 5. *Frequency of the depth of the mixing layer in each category of atmospheric stability*

Atmospheric Stability	A		B		C		D		E		F	
*MH Range	Freq.	Perc.%	Freq.	perc.%	Freq.	perc.%	Freq.	perc.%	Freq.	perc.%	Freq.	perc.%
0–500	0	0	1	0	0	0	50	2	1390	86	1724	88
500–700	0	0	19	1	0	0	9	0	15	1	73	4
700–900	0	0	30	2	10	1	17	1	5	0	73	4
900–1100	0	0	60	4	96	11	98	4	71	4	89	5
1100–1300	0	0	32	2	88	10	195	8	46	3	0	0
1300–1500	0	0	17	1	123	15	468	20	52	3	0	0
1500–1700	8	2	154	10	96	11	321	14	29	2	0	0
1700–1900	34	7	244	16	112	13	335	14	1	0	0	0
1900–2100	55	12	446	30	209	25	294	12	0	0	0	0
2100–2300	91	19	292	19	86	10	247	10	0	0	0	0
2300–2500	112	24	198	13	6	1	110	9	0	0	0	0
2500–2700	92	19	8	1	9	1	72	3	0	0	0	0
2700–2900	79	17	1	0	3	0	43	2	0	0	0	0
> 2900	4	1	2	0	4	0	105	0	0	0	0	0
No of data	475		1504		842		2368		1609		1959	

*MH = Mixing Height, Freq. = frequency, Perc. = Percent

Fig. 7. *Mixing height bands arranged according to wind speed: (> 5), (5–2), and (> 2) m/s*

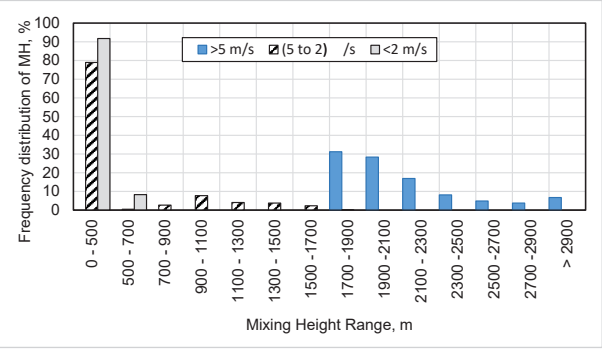

less than 700 m. However, more than 90% of the values are less than 500 m for wind speeds ranging from 5 m/s to 2 m/s.

Analysis of sandstorms in the study area

The hourly sandstorms are investigated based on the modelled atmospheric stability and height of the mixing layer as given in *Table 6*. The recorded total hours of sandstorms estimated as 376 during the study year 2019. Neutral conditions were dominant with the frequency of occurrence 42% of the total sandstorm events. Very unstable conditions registered a very low frequency of occurrence during sandstorms (4.5%) with a relatively low average wind speed (1.8 m/s). During night hours, the height of the mixing layer was 14% less than 350 m and 16% less than 180 m, which increases the concentration of fine sand on the ground surface. The events of sandstorms along four decades were also statistically analysed. The average hourly events of sandstorms were 476 hours per year. The maximum events of sandstorms were recorded in the year 2009 with total sandstorm hours 1338, while the minimum events were 50 hours in year 1995. The trend of sandstorms is not existing according to year variation. More studies are required to investing the concentration and mineralogy of the deposited sand during the storms and it is related to the atmospheric stability conditions and mixing height.

Meteorological conditions i.e., temperature, wind speed, wind direction, and humidity were investigated during sandstorm hours along the period from 1980

Table 6. *Average mixing height, temperature, and wind speed during sandstorm hours over year 2019 based on modelled atmospheric stability conditions*

Stability	Wind speed, m/s	Temperature, °C	Humidity, %	Average mixing height, m	No of sandstorm hours	Frequency of hourly handstorm, %
A	1.8	23.5	46.8	1877	17	4.5
B	3.1	21.8	44.4	1563	54	14.4
C	6.1	24.4	39.7	1777	36	9.6
D	7.0	22.3	50.9	1626	159	42.3
E	3.5	18.1	57.9	349	51	13.6
F	1.8	14.7	64.4	182	59	15.7

to 2019 as presented in *Fig. 8*. The average estimated wind speed was 5.5 ± 0.75 m/s while the average temperature was 26.25 ± 2°C. The weather during sandstorms features moderate wind speed and temperatures. From *Fig. 8*, we note that humidity has increased, and the average temperature has relatively decreased in the last decade. This change is due to the increase of agricultural activity in the last ten years around the study area (Al-Wabel et al., 2020).

Wind direction during sandstorms was also investigated over the last four decades using wind rose graphic as shown in *Fig. (9)*. It was surprising that the direction of wind during sandstorms was restricted between narrow ranges where it was blowing between 135° to 235° from the north with the majority (75% of the values) to the south (±22.5 degree) as illustrated in the figure. Cultivation of dense and tall trees in the south of the study area will decrease the severity of sandstorms in the future.

Fig. 8. *Average values of temperature, humidity, and wind speed over four decades during sandstorm hours*

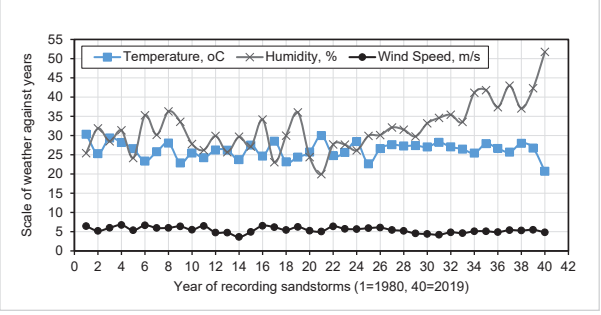

Fig. 9. *Wind rose diagram for wind speed and its direction during sandstorms*

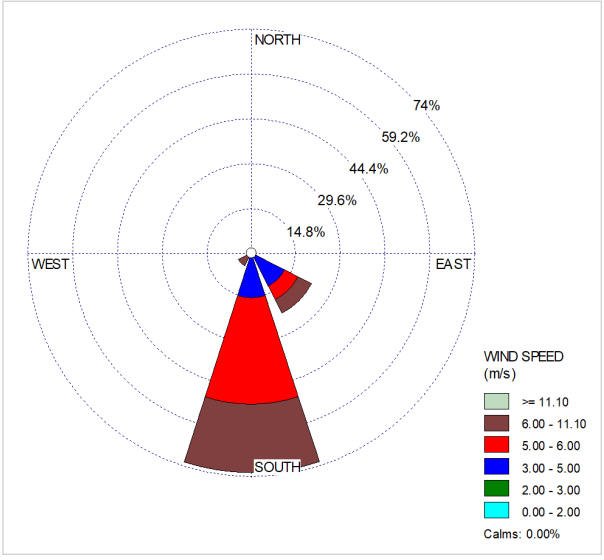

Conclusion

The precise determination of atmospheric stability conditions is very important in the estimation of the transport and deposition of pollutants. A MATLAB code was applied to estimate the hourly classes of atmospheric stability and the height of the mixing layer in Qassim region, KSA, in 2019. The developed model used hourly surface weather data and incoming solar radiation to express the amount of insolation strength required to determine the atmospheric stability conditions according to Pasquill-Gifford classes. Based on the suggested incoming solar radiation and the wind

speed range, the model determines the Pasquill-Gifford atmospheric stability categories and heights of the mixing layer in the study area. The results show that the atmosphere is mostly unstable during daytime hours with a frequency of 66.7% for all observed times. It was also observed that the frequency of neutral conditions on winter days was greater than that on summer days. The occurrence of stable categories in summer and winter nights was nearly equal, with a frequency of 60%. The hourly heights of mixing layers were calculated using a modified MATLAB code based on the results of atmospheric stability conditions and the measured surface weather data. The results indicated that nocturnal mixing height values ranged from 300 m to 700 m in all seasons. From these results, we can conclude that the study area features high mixing layers compared with other sites in the world. This result also indicates that extremely stable conditions occur during the night-time hours and that an inversion layer exists. The inversion layer obstructs the dispersion of contaminants that increases the concentrations of deposited contaminants at receptors. Mechanical turbulence by wind is dominant during night-time hours; this fact is obvious during spring season, where wind speed is greater than in other seasons, which is compatible with the estimated mixing height values.

The study area suffers from the blowing of sandstorms. This fact is obvious from the statistical analysis of sandstorms events over 40 years. While increasing the activity of cultivation over the last ten years increases the humidity and decreases the temperature within the study area. This change in the activity may decrease the severity of sandstorms in the future. Low values of mixing heights increase the sand concentration during storms on the ground surface, particularly at night hours. Wind direction during sandstorms is restricted within a narrow zone around the south direction. We strongly recommend cultivating heavy and tall trees in this direction that will protect the study area from sandstorms in the future.

References

Abolkhair, Y. M. S. (1986). The statistical analysis of the sand grain size distribution of Al-Ubay-lah barchan dunes, northwestern Ar-Rub-Alkhali Desert, Saudi Arabia. GeoJournal, 13(2), 103-109. https://doi.org/10.1007/BF00212712

Al-Wabel, M. I., Sallam, A., Ahmad, M., Elanazi, K., & Usman, A. R. A. (2020). Extent of Climate Change in Saudi Arabia and Its Impacts on Agriculture: A Case Study from Qassim Region. In Environment, Climate, Plant and Vegetation Growth (pp. 635-657). Springer. https://doi.org/10.1007/978-3-030-49732-3_25

Albaqami, S. (2020). Spatial and temporal analysis of dust storms in Saudi Arabia and associated impacts, using Geographic Information Systems and remote sensing.

Albugami, S., Palmer, S., Cinnamon, J., & Meersmans, J. (2019). Spatial and temporal variations in the incidence of dust storms in saudi arabia revealed from in situ observations. Geosciences, 9(4), 162. https://doi.org/10.3390/geosciences9040162

Alharbi, A. B., & Gomaa, F. A. (2014). Physio-chemical properties of airborne particles collected from some locations in Qassim region. Life Science Journal, 11(9), 1031.

Arya, S. P. S. (1981). Parameterizing the height of the stable atmospheric boundary layer. Journal of Applied Meteorology and Climatology, 20(10), 1192-1202. https://doi.org/10.1175/1520-0450(1981)020<1192:PTHOTS>2.0.CO;2

Baklanov, A. (2004). Parameterisation of SBL height in atmospheric pollution models. In Air Pollution Modeling and Its Application XV (pp. 415-424). Springer.https://doi.org/10.1007/0-306-47813-7_42

Barratt, R. (2002). Atmospheric Dispersion Modeling. An Introduction to Practical Applications.

Beegum, S. N., Gherboudj, I., Chaouch, N., Temimi, M., & Ghedira, H. (2018). Simulation and analysis of synoptic scale dust storms over the Arabian Peninsula. Atmospheric Research, 199, 62-81. https://doi.org/10.1016/j.atmosres.2017.09.003

Benkley, C. W., & Schulman, L. L. (1979). Estimating hourly mixing depths from historical meteorological data. Journal of Applied Meteorology, 18(6), 772-780. https://doi.org/10.1175/1520-0450(1979)018<0772:EHMDFH>2.0.CO;2

Brokamp, C., Brandt, E. B., & Ryan, P. H. (2019). Assessing exposure to outdoor air pollution for epidemiological studies: Model-based and personal sampling strategies. Journal of Allergy and Clinical Immunology, 143(6), 2002-2006. https://doi.org/10.1016/j.jaci.2019.04.019

Butt, M. J., & Mashat, A. S. (2018). MODIS satellite data eval-

uation for sand and dust storm monitoring in Saudi Arabia. International Journal of Remote Sensing, 39(23), 8627-8645. https://doi.org/10.1080/01431161.2018.1488293

Gifford Jr, F. A. (1961). Use of routine meteorological observations for estimating atmospheric dispersion. Nuclear Safety, 2, 47-51.

Honnert, R., Efstathiou, G. A., Beare, R. J., Ito, J., Lock, A., Neggers, R., Plant, R. S., Shin, H. H., Tomassini, L., & Zhou, B. (2020). The atmospheric boundary layer and the "gray zone" of turbulence: A critical review. Journal of Geophysical Research: Atmospheres, 125(13), e2019JD030317. https://doi.org/10.1029/2019JD030317

Hutter, K., Wang, Y., & Chubarenko, I. P. (2011). The Role of the Earth's Rotation: Fundamentals-Rotation and Stratification Influenced Dynamics. In Physics of Lakes (pp. 1-48). Springer. https://doi.org/10.1007/978-3-642-19112-1_11

Latini, G., Grifoni, R. C., & Passerini, G. (2000). Dependency of mixing height as function of Monin-Obukhov length on stability conditions. WIT Transactions on Ecology and the Environment, 42.

Levi, Y., Dayan, U., Levy, I., & Broday, D. M. (2020). On the association between characteristics of the atmospheric boundary layer and air pollution concentrations. Atmospheric Research, 231, 104675. https://doi.org/10.1016/j.atmosres.2019.104675

Modaihsh, A., Ghoneim, A., Al-Barakah, F., Mahjoub, M., & Nadeem, M. (2017). Characterizations of Deposited Dust Fallout in Riyadh City, Saudi Arabia. Polish Journal of Environmental Studies, 26(4). https://doi.org/10.15244/pjoes/68565

Morbidelli, R., Corradini, C., Saltalippi, C., & Flammini, A. (2011). Atmospheric Stability and Meteorological Scenarios as Inputs to Air Pollution Transport Modeling. Water, Air, & Soil Pollution, 218(1 LB-Morbidelli2011), 275-281. https://doi.org/10.1007/s11270-010-0640-5

Rabeiy, R. E. (2010). Spatial Modeling of Heavy Metal Pollution of Forest Soils in a Historical Mining Area Using Geostatistical Methods and Air Dispersion Modeling. Papierflieger-Verlag.

Samarkandi, O. A., Khan, A. A., Alazmy, W., Alobaid, A. M., & Bashatah, A. S. (2017). The pulmonary consequences of sandstorms in Saudi Arabia: a comprehensive review and update. Am J Disaster Med, 12, 179-188. https://doi.org/10.5055/ajdm.2017.0272

Schumann, U. (1988). Minimum friction velocity and heat transfer in the rough surface layer of a convective boundary layer. Boundary-Layer Meteorology, 44(4), 311-326. https://doi.org/10.1007/BF00123019

Schutt, M., Seim, H., & Ieee. (2015). Impact of Stability on the Atmospheric Boundary Layer. In Oceans 2015 - Mts/Ieee Washington. https://doi.org/10.23919/OCEANS.2015.7401821

Soltan, M.-E., Al-Ayed, A., & Ismail, M. (2020). Evaluation of the concentrations of some metallic elements in the fallen dust extractants on the Ar Rass city, Qassim region, KSA. International Journal of Environmental Analytical Chemistry, 1-16. https://doi.org/10.1080/03067319.2020.1811264

Tanamachi, R. L., Frasier, S. J., Waldinger, J., LaFleur, A., Turner, D. D., & Rocadenbosch, F. (2019). Progress toward characterization of the atmospheric boundary layer over northern Alabama using observations by a vertically pointing, S-band profiling radar during VORTEX-Southeast. Journal of Atmospheric and Oceanic Technology, 36(11), 2221-2246. https://doi.org/10.1175/JTECH-D-18-0224.1

Tangborn, A., Demoz, B., Carroll, B. J., Santanello, J., & Anderson, J. L. (2020). Assimilation of lidar planetary boundary layer height observations. Atmospheric Measurement Techniques Discussions, 1-19. https://doi.org/10.5194/amt-2020-238

Wang, L., Liu, J., Gao, Z., Li, Y., Huang, M., Fan, S., Zhang, X., Yang, Y., Miao, S., & Zou, H. (2019). Vertical observations of the atmospheric boundary layer structure over Beijing urban area during air pollution episodes. Atmospheric Chemistry and Physics, 19(10), 6949-6967. https://doi.org/10.5194/acp-19-6949-2019

Yu, T.-W. (1978). Determining height of the nocturnal boundary layer. Journal of Applied Meteorology, 17(1), 28-33. https://doi.org/10.1175/1520-0450(1978)017<0028:DHOTNB>2.0.CO;2

Zaïdi, H., Dupont, E., Milliez, M., Carissimo, B., & Musson-Genon, L. (2014). Effect of Atmospheric Stability on the Atmospheric Dispersion Conditions Over a Industrial Site Surrounded by Forests. In D. G. Steyn, P. J. H. Builtjes, & R. M. A. Timmermans (Eds.), Air Pollution Modeling and its Application XXII (pp. 733-737). Springer Netherlands. LB - Zaïdi2014 https://doi.org/10.1007/978-94-007-5577-2_124